Filamin B represses chondrocyte hypertrophy in a Runx2/Smad3-dependent manner

Lihua Zheng,[1,2] Hwa-Jin Baek,[1] Gerard Karsenty,[2] and Monica J. Justice[1]

[1]Department of Molecular and Human Genetics, Baylor College of Medicine, Houston, TX 77030
[2]Department of Genetics and Development, Columbia University, College of Physicians and Surgeons, New York, NY 10032

FILAMIN B, which encodes a cytoplasmic actin binding protein, is mutated in several skeletal dysplasias. To further investigate how an actin binding protein influences skeletogenesis, we generated mice lacking intact Filamin B. As observed in spondylocarpotarsal synostosis syndrome patients, Filamin B mutant mice display ectopic mineralization in many cartilaginous elements. This aberrant mineralization is due to ectopic chondrocyte hypertrophy similar to that seen in mice expressing Runx2 in chondrocytes. Accordingly, removing one copy of *Runx2* rescues the *Filamin B* mutant phenotype, indicating that Filamin B is a regulator of Runx2 function during chondrocyte differentiation. Filamin B binds Smad3, which is known to interact with Runx2. Smad3 phosphorylation is increased in the mutant mice. Thus, Filamin B inhibits Runx2 activity, at least in part, through the Smad3 pathway. Our results uncover the involvement of actin binding proteins during chondrogenesis and provide a molecular basis to a human genetic disease.

Introduction

Skeletogenesis occurs through two mechanisms: intramembranous ossification and endochondral ossification (Karsenty and Wagner, 2002). During intramembranous ossification, which occurs in some cranial bones and the clavicle, mesenchymal cells differentiate directly into osteoblasts without a chondrocyte intermediary step. In endochondral bone formation, mesenchymal cells first condense to shape the future skeletal elements. The mesenchymal cells within these condensations differentiate into chondrocytes, which express α1(II) collagen, whereas the α1(I) collagen–expressing undifferentiated mesenchymal cells at the periphery of the condensations form the perichondrium. After the formation of the cartilaginous templates, chondrocytes further differentiate into prehypertrophic chondrocytes and then into hypertrophic chondrocytes, which express α1(X) collagen. Terminally differentiated hypertrophic chondrocytes also express matrix metalloproteinase 13 (Mmp13; also called collagenase 3). This hypertrophic chondrocyte differentiation step does not occur in skeletal elements that are destined to be permanent cartilage. Finally, the osteoblasts in the perichondrium invade the hypertrophic chondrocyte area and deposit bone matrix.

Correspondence to Monica J. Justice: mjustice@bcm.tmc.edu

Abbreviations used in this paper: E, embryonic day; ES, embryonic stem; *Ihh, Indian hedgehog*; *Mmp13, matrix metalloproteinase 13*; P, postnatal day; *Ppr, parathyroid hormone–related peptide receptor*; SSS, spondylocarpotarsal synostosis syndrome.

The online version of this article contains supplemental material.

Skeletogenesis is tightly controlled by transcription factors. Among them, Runx2, a transcription factor containing a *runt* DNA binding domain, is a key gene for osteoblast differentiation (Ducy et al., 1997). In addition, Runx2 plays multiple and opposite roles during chondrogenesis (Takeda et al., 2001; Komori, 2002; Hinoi et al., 2006). On one hand, Runx2 is transiently expressed in prehypertrophic chondrocytes, where it, in conjunction with Runx3 for some skeletal elements, is necessary to initiate chondrocyte hypertrophy (Yoshida et al., 2004), the ultimate event of chondrogenesis. Accordingly, Runx2 constitutive expression in nonhypertrophic chondrocytes leads to premature and ectopic chondrocyte hypertrophy and, thereby, bone formation (Takeda et al., 2001). On the other hand, through its perichondrial expression, Runx2 prevents chondrocyte maturation (Hinoi et al., 2006). To date, histone deacetylase 4 (HDAC4) is the only protein known to regulate Runx2 function during chondrogenesis (Vega et al., 2004). This contrasts sharply with the larger number of molecules regulating Runx2 function during osteogenesis (Bialek et al., 2004; Kronenberg, 2004; Komori, 2006) and suggests that additional regulators of Runx2's ability to favor chondrocyte hypertrophy may exist.

Filamins are a family of large cytoplasmic actin binding proteins that cross-link filamentous actin into a three-dimensional network (Stossel et al., 2001). The family consists of three members in mammals, Filamin A, B, and C (Flna, Flnb, and Flnc). All three members share well-conserved actin binding domains and a rodlike domain of 24 repeats, which is interrupted

The Journal of Cell Biology, Vol. 178, No. 1, July 2, 2007 121–128
http://www.jcb.org/cgi/doi/10.1083/jcb.200703113

by two poorly conserved hinge domains (Popowicz et al., 2006). All three members are widely expressed, although Flnc is more restricted to skeletal and cardiac muscle (Feng and Walsh, 2004). Studies in different model organisms indicate that Filamins may interact with >30 proteins, thus implicating them in many cellular functions ranging from mechanical stability, to cell–cell and cell–matrix interactions, to integrators of signal transductions (Stossel et al., 2001; van der Flier and Sonnenberg, 2001; Popowicz et al., 2006).

Genetic evidence indicates that Filamins are essential for the development of multiple organs in human, including skeleton (Robertson et al., 2003; Krakow et al., 2004). For instance, mutations in *Flnb* are found in five human skeletal disorders: spondylocarpotarsal synostosis syndrome (SSS), Boomerang dysplasia, atelosteogenesis I, atelosteogenesis III, and Larsen syndrome (Krakow et al., 2004). The recessive SSS, characterized by short stature and fusions of vertebral, carpal, and tarsal bones, is caused by stop codon mutations within rod domain repeats, whereas the other dominant disorders are associated with missense mutations or small in-frame deletions. Patients with Boomerang dysplasia (Bicknell et al., 2005) have underossification of the limb bones and vertebrae. Atelosteogenesis I and III (Farrington-Rock et al., 2006) patients have vertebral abnormalities, disharmonious skeletal maturation, hypoplastic long bones, and joint dislocations. Patients with Larsen syndrome (Zhang et al., 2006) have multiple joint dislocations, craniofacial abnormalities, and accessory carpal bones. The molecular mechanisms whereby mutations in *Flnb* result in skeletal abnormalities remain unknown.

To study how *Flnb* mutations could lead to skeletal disorders, we generated mice deficient in full-length Flnb protein and found that the mutant mice display a phenotype similar to the recessive SSS. Cellular and histological analysis showed that these defects are due to premature and/or ectopic chondrocyte hypertrophy in skeletal elements that should be permanent cartilage. Molecular studies showed that these abnormalities are due to an increase in Runx2 activity. Here, we also show that Flnb does not interact with either Runx2 or HDAC4 but can bind to Smad3, a protein expressed in prehypertrophic chondrocytes and able to interact with Runx2 (Sakou et al., 1999; Kang et al., 2005). These results demonstrate for the first time that Flnb can influence the function of a transcription factor, identify a new mechanism whereby Runx2's function during chondrogenesis is regulated, and provide a molecular basis for SSS.

Results

Flnb mutant mice display ectopic mineralization

The *Flnb* gene trap embryonic stem (ES) cell line contains a β-galactosidase neomycin insertion within the 20th intron of *Flnb* (Fig. 1 A; see Materials and methods). The 20th exon of *Flnb* splices into the insertion to generate a fusion transcript, but it does not produce any wild-type transcript (Fig. 1 C and Fig. S1, available at http://www.jcb.org/cgi/content/full/jcb.200703113/DC1). The mutant transcript is predicted to encode a truncated Flnb protein of 1,624 of the full-length 2,602 amino acids and to be fused with *β-galactosidase* (Fig. 1 D). Intercrosses of *Flnb*

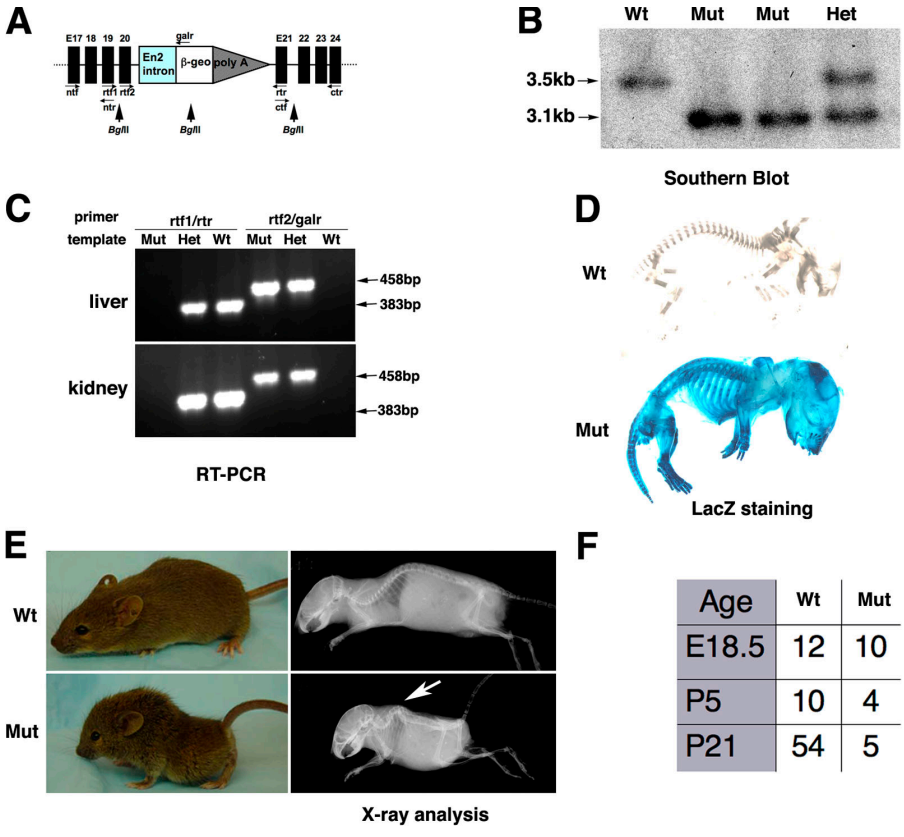

Figure 1. **Generation of *Flnb* mutant mice.** (A) The gene trap ES cell line contains a *β-geo* insertion within the 20th intron of *Flnb* gene. BglII, which has a single restriction site within the insertion, was used to digest genomic DNA for genotyping. The exact locations of the primers used for genotyping and RT-PCRs are indicated by the arrows. (B) Southern blotting detects a mutant band of 3.1 kb and a wild type of 3.5 kb. (C) RT-PCR analysis shows no full-length *Flnb* gene expression in the homozygous mutants. The rtf1/rtr primer pair amplifies the wild-type *Flnb* transcript spanning the *β-geo* insertion. The rtf2/galr primer pair amplifies the fusion transcript of the *Flnb* and *β-geo* insertion. Total RNA from the liver and kidney of each genotyped mouse was used as the template. (D) A Flnb–β-galactosidase fusion protein is present in the mutant mice at P0 as shown by LacZ staining. (E) The surviving homozygous mutant mouse is smaller compared with a wild-type littermate and has severe kyphosis (arrow), indicated by x-ray analysis at P30. (F) *Flnb* mutants die postnatally. At P5 and P21, fewer than the expected numbers of homozygotes are observed. At E18.5, the numbers of each genotype are consistent with Mendelian segregation.

heterozygotes in the 129/Ola-C57BL/6 mixed genetic background generate homozygous *Flnb* mice at Mendelian ratios at embryonic day (E) 18.5 (Fig. 1 F). However, at postnatal day (P) 5 or P21, the number of homozygous mutants is 50 and 90% decreased, respectively. The few surviving homozygous mutants are runted and have abnormal postures, with x-ray analysis showing severe kyphosis (Fig. 1 E). All these features are reminiscent of the clinical manifestation of SSS (Krakow et al., 2004).

Staining of skeletal preparations with Alizarin red for mineralized ECM and Alcian blue for unmineralized cartilaginous ECM reveals multiple skeletal defects in the *Flnb* mutants. For instance, similar to what is seen in SSS patients, homozygous mice have both cervical vertebrae and carpal bone fusions. Indeed, although in wild-type P30 mice, unmineralized cartilaginous ECM separates the seven cervical vertebrae, the intervertebral ECM of the mutant mice was stained by Alizarin red, indicating that this ECM was mineralized, causing vertebral fusions (Fig. 2 A). In P0 mutant mice, mineralization of the cartilage ECM, although detectable, is less extensive, suggesting that the fusion of cervical vertebrae develops progressively. The mineralization of intervertebral ECM was first detectable at E17.5, whereas no difference in cervical vertebrae staining was seen between wild type and mutant at E16.5, suggesting that the cartilage develops properly in the homozygous mutants but becomes mineralized (Fig. 2 A). In addition, the cartilage that would normally separate carpal bones in the wild-type mice is ectopically mineralized in the mutant mice. At P0, blue staining cartilaginous ECM separates the carpal bones, whereas by P15, this ECM is becoming mineralized, leading to fusions of carpal bones (Fig. 2 B).

Homozygous *Flnb* mutant mice also display abnormal ossification in the chondrocostal cartilage of the rib cage and sterna. In wild-type mice at all stages examined, chondrocostal cartilage and cartilage separating the sternebrae never ossify and are stained by Alcian blue. In contrast, in homozygous mutant mice, although the chondrocostal cartilage is stained with Alcian blue at P0, it stains progressively with Alizarin red at P15 and P30, indicating that this ECM is becoming prematurely mineralized (Fig. 3 A). Similarly, cartilaginous areas between sternebrae become mineralized in the mutant mice. Collectively, these ectopic ECM mineralization processes observed in cervical, carpal, and rib cage suggest that one of the Flnb functions is to regulate chondrocyte differentiation.

Ectopic mineralization in Flnb mutant mice is due to ectopic chondrocyte differentiation

To determine if this ectopic mineralization was caused by ectopic chondrocyte hypertrophy, we analyzed the expression of molecular markers of proliferating, prehypertrophic, and hypertrophic chondrocytes in ribs by in situ hybridization. We used probes to *α1(II) collagen*, a gene expressed in proliferating and prehypertrophic chondrocytes; *Indian hedgehog* (*Ihh*) and *parathyroid hormone–related peptide receptor* (*Ppr*), two prehypertrophic chondrocyte markers; *α1(X) collagen*, a marker of hypertrophic chondrocytes; *Mmp13*, a terminally differentiated hypertrophic marker; and *α1(I) collagen*, which is expressed in osteoblasts and mesenchymal cells in the bone collar. At P0, although *α1(II) collagen* is expressed in the cartilage area between sternebrae 3/4 of wild-type mice, its expression cannot be detected in mutant mice (Fig. 3 B). Instead, the *Flnb*^{mut} cells express *α1(X) collagen* and *Mmp13* (Fig. 3 C), indicating that the chondrocytes have differentiated into hypertrophic chondrocytes. Similarly, *α1(II) collagen* is expressed in the cartilaginous area between sternebrae 2/3 of P0 in wild-type mice, but its expression at this location is diminished in mutant mice. Instead, these cells express *Ihh*, *Ppr*, and *α1(X) collagen*. These results indicate that the chondrocytes within that area are undergoing hypertrophy in the homozygous mutant mice at P0

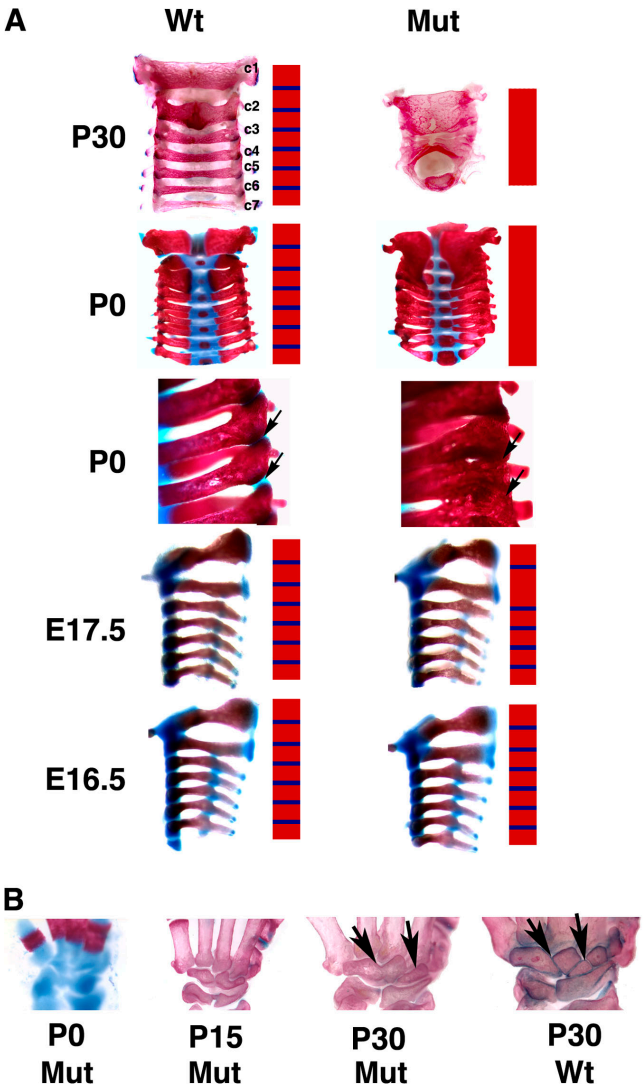

Figure 2. **Skeletal defects in *Flnb* mutant mice similar to human spondylocarpotarsal syndrome.** (A) Ectopic ECM mineralization in the cervical vertebrae of the *Flnb* mutants. In wild-type mice, seven cervical vertebrae are separated by blue staining cartilaginous ECM at all stages. In the P30 and P0 homozygous mutants, the cervical vertebrae are fused (arrows) with the absence of blue staining cartilage in between. The cervical fusion phenotype appears at E17.5, as the blue staining cartilage between cervical vertebrae 2 and 3 is replaced by red staining mineralized ECM. No fusions are visible at E16.5 in the homozygous mutants. (B) Ectopic ECM mineralization in the carpal bones of the *Flnb* mutants. In wild-type mice, bones are separated by blue staining cartilaginous ECM (arrows). In the P30 and P15 mutants, carpal bones are fused with little or no blue staining cartilage in between. At P0, the cartilage appears to be normal in mutant mice.

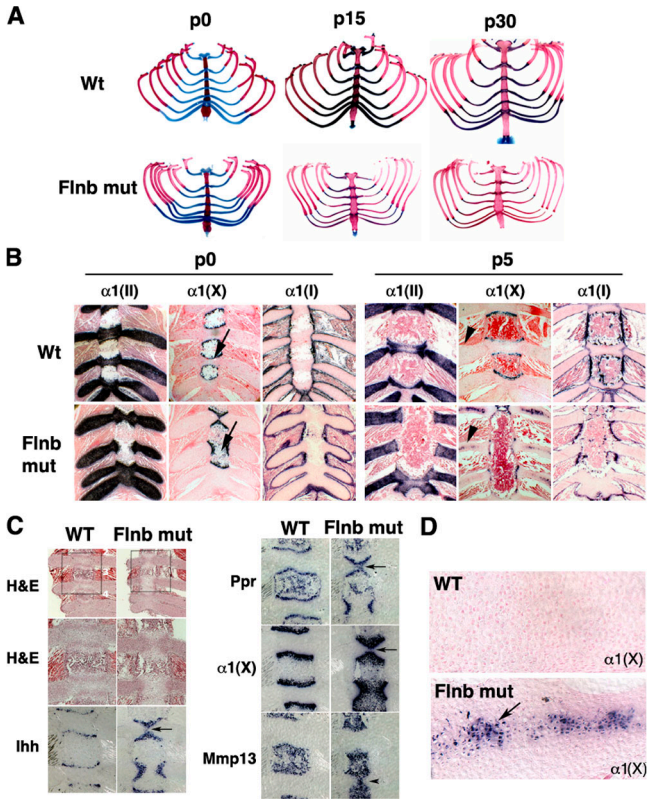

Figure 3. **Ectopic ECM mineralization is caused by abnormal chondrocyte differentiation in the *Flnb* mutants.** (A) Ectopic ECM mineralization in ribs. In wild-type mice, the four sternebrae are separated by blue staining cartilage and the chondrocostal cartilage remains blue at all stages. In homozygous mutant mice, sternebrae 3 and 4 are already fused without blue staining cartilage in between. The cartilage between sternebrae 2 and 3 is undergoing mineralization at P0 and completely mineralized with red staining by P15. The chondrocostal cartilage of the mutant mice is stained blue at P0 and partly stained red at P15 and P30. (B) In situ hybridizations with collagen markers. At P0, in wild-type ribs, chondrocytes between sternebrae 2 and 3, as well as those between sternebrae 3 and 4, express *α1(II) collagen*. In mutant ribs, chondrocytes between sternebrae 3 and 4 do not express *α1(II) collagen* and have already become mineralized. Meanwhile, chondrocytes between sternebrae 2 and 3 are expressing *α1(X) collagen* in the middle and are undergoing hypertrophy. At P5, in the wild-type rib, the chondrocytes between sternebrae 2 and 3, as well as those between sternebrae 3 and 4, still express *α1(II) collagen*. In addition, chondrocytes within the chondrocostal cartilage do not express *α1(X) collagen*. However, in mutant ribs, *α1(X) collagen* can be readily detected within the chondrocostal chondrocytes. Furthermore, chondrocytes between sternebrae 2 and 3 do not express *α1(II) collagen* and instead are now completely mineralized. At both P0 and P5, no difference is seen in the *α1(I) collagen*–expressing bone collar between the wild-type and mutant mice. The arrows point to the cartilage between sternebrae 3/4, and arrowheads point to the chondrocostal cartilage. (C) Ectopic chondrocyte hypertrophy in the cartilage between sternebrae at P0. In wild-type ribs, chondrocytes separate the sternebrae 2/3 and 3/4. In mutant ribs, chondrocytes are becoming hypertrophic between sternebrae 2/3, as indicated by the expression of *Ihh*, *Ppr*, and *α1(X) collagen* in the mutants. The area between sternebrae 3/4 is becoming mineralized, as indicated by the expression of *Mmp13*. The arrows point to the cells between sternebrae 2/3 and the arrowhead points to the cells between sternebrae 3/4. (D) Magnified cellular phenotype in the chondrocostal cartilage at P5. The chondrocytes in the middle of the cartilage are enlarged and expressing *α1(X) collagen* prematurely in the mutants. *α1(I) collagen* is an osteoblast marker, *α1(II) collagen* is a proliferating and prehypertrophic chondrocyte marker, *α1(X) collagen* is a hypertrophic chondrocyte marker, *Ihh* is a prehypertrophic chondrocyte marker, *Ppr* is a prehypertrophic chondrocyte marker, and *Mmp13* is a terminally differentiated hypertrophic marker. The arrows point to hypertrophic chondrocytes.

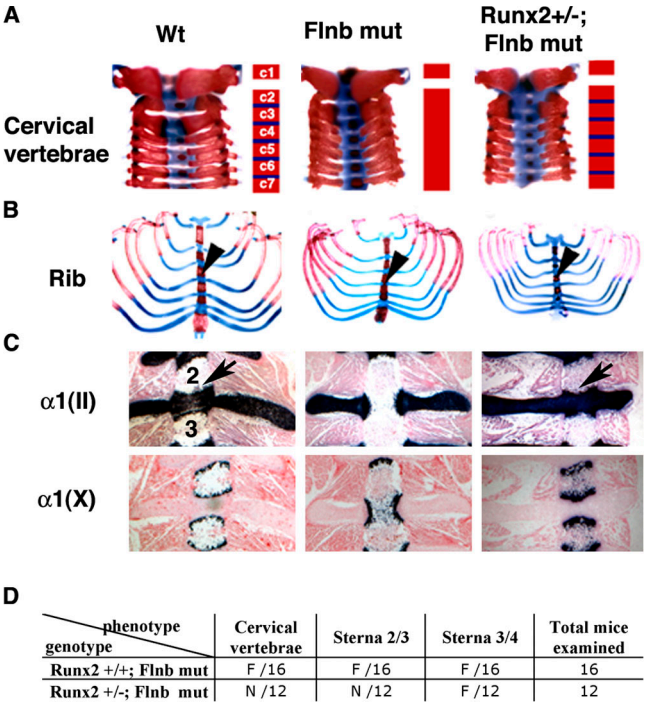

D

phenotype / genotype	Cervical vertebrae	Sterna 2/3	Sterna 3/4	Total mice examined
Runx2 +/+; Flnb mut	F /16	F /16	F /16	16
Runx2 +/-; Flnb mut	N /12	N /12	F /12	12

Figure 4. **Genetic interaction between *Runx2* and *Flnb*.** (A and B) Skeletal preparations of cervical vertebrae and rib cage, respectively, at P0. The rectangular bars illustrate the mineralized (red) and the unmineralized (blue) ECM in cervical vertebrae. In wild-type mice, seven cervical vertebrae and four sternebrae are separated by blue staining cartilage. In $Flnb^{mut}$ mice, the cervical vertebrae are extensively fused and the cartilage is ectopically mineralized. In $Runx2^{+/-}$; $Flnb^{mut}$ mice, the cervical vertebrae are separated by blue staining ECM. The blue staining cartilage between sternebrae 2/3 is also restored, although the cartilage between sternebrae 3/4 is still missing. The arrowheads point to intervertebral discs between sternebrae 2/3. (C) In situ hybridization analysis of *α1(II) collagen* and *α1(X) collagen* expression in ribs. In wild-type and $Runx2^{+/-}$; $Flnb^{mut}$ mice, sternebrae 2/3 is separated by *α1(II) collagen*–expressing chondrocytes. However, in $Flnb^{mut}$ mice, *α1(X) collagen* but no *α1(II) collagen* is expressed in the area between sternebrae 2/3. The skeletal elements were stained with alcian blue and alizarin red. The arrows refer to the cartilage between sternebrae 2/3. (D) Statistics on the rescue experiment. The cervical vertebrae fusion phenotype is completely rescued after removing one copy of *Runx2*; the same is true for the fusion between sternebrae 2 and 3. The fusion between sternebrae 3 and 4 is not rescued. F, fusion of bone elements; N, normal bone elements.

(Fig. 3 C). At P5, *α1(II) collagen* is no longer expressed in the cartilage area between sternebrae 2/3 and 3/4, but osteoblasts are present, as demonstrated by the expression of *α1(I) collagen* (Fig. 3 B). This observation explains the presence of ectopic bone formation in the sterna.

At P0, cells of both wild-type and $Flnb^{mut}$ chondrocostal cartilage express *α1(II) collagen* but not *α1(X) collagen*, indicating that chondrocytes in the chondrocostal cartilage are not hypertrophic (Fig. 3 B). However, 5 d later, *α1(X) collagen* expression can be detected in the chondrocostal cartilage of the homozygous mutant mice, suggesting that hypertrophic chondrocyte differentiation has occurred (Figs. 3, B and D). Collectively, these results reveal that there is uncontrolled differentiation of chondrocytes into hypertrophic chondrocytes in the $Flnb^{mut}$ chondrocostal cartilage, a cellular abnormality reminiscent of what was seen in mice overexpressing Runx2 in chondrocytes (*α1[II]-Runx2* transgenic mice; Takeda et al., 2001).

Genetic interaction between Flnb and Runx2

The similarity between *Flnb* mutant and *α1(II)-Runx2* phenotypes suggests that Flnb and Runx2 may interact genetically, with Flnb acting as a negative regulator of Runx2 activity. To test this hypothesis, we generated *Flnb* mutant mice on a *Runx2* haploinsufficiency background and examined them for ectopic mineralization. Remarkably, $Runx2^{+/-}$; $Flnb^{mut}$ mice have completely normal cervical vertebrae (Fig. 4 A), and the sterna phenotype observed in $Flnb^{mut}$ mice is partially rescued (Fig. 4 B). Accordingly, normal expression of *α1(II)* and *α1(X)* was restored in $Runx2^{+/-}$; $Flnb^{mut}$ mice (Fig. 4 C). The rescue, complete or partial, is always fully penetrant (Fig. 4 D). These results provide genetic evidence that Flnb and Runx2 interact and suggest that Flnb regulates chondrocyte hypertrophy by inhibiting Runx2 activity.

Flnb inhibits Runx2 by regulating Smad3 phosphorylation

How does a cytoplasmic molecule like Flnb inhibit the function of a nuclear transcription factor like Runx2? We were unable to detect mislocalization of Runx2 and HDAC4 proteins in the *Flnb* mutants or to identify biochemical interactions between Flnb and Runx2 or HDAC4 (Fig. 5, A and B; and Fig. S2, available at http://www.jcb.org/cgi/content/full/jcb.200703113/DC1). Although negative and therefore to be interpreted cautiously, these observations suggest that Flnb must interact with another protein.

Filamin A, another member of the Filamin protein family, has been shown to bind CBFβ, a nuclear factor that can interact with Runx proteins. Through this interaction, Filamin A prevents CBFβ from entering the nucleus to activate the Runx1 transcription factor (Yoshida et al., 2005). Therefore, we examined whether Flnb also binds CBFβ. We failed, however, to detect any interaction between Flnb and CBFβ (Fig. 5 C), nor could we see abnormal intracellular localization of CBFβ in chondrocytes (Fig. S2). Thus, the Runx2 interaction with Flnb appears to be CBFβ independent under the conditions of these assays.

Deletion of a phosphorylation site on Smad3 causes ectopic chondrocyte hypertrophy, suggesting that TGF-β–Smad3 signals repress chondrocyte differentiation (Ferguson et al., 2000; Yang et al., 2001). Because phosphorylated Smad3 has been shown to recruit HDAC4 to inhibit Runx2 activity in osteoblasts by forming a HDAC4–Smad3–Runx2 complex (Kang et al., 2005), we tested whether Flnb could repress Runx2 activity by interacting with Smad3. Indeed, three lines of evidence support the notion that a direct interaction between Flnb and Smad3 exists. First, Smad3 can be immunoprecipitated with Flnb in an in vitro overexpression assay (Fig. 5 D). Notably, compared with Smad3, Smad2 and -5 show no detectable interaction with Flnb (Fig. 5, E and F), although an interaction with Smad4 and -6 is also detected (Fig. S2). Second, endogenous Smad3 protein can be immunoprecipitated by tagged Flnb protein (Fig. 5 G). Third, Flnb directly interacts with Smad3 in a pull-down assay (Fig. 5, H and I). Because the phosphorylation of Smad3 is important in chondrocyte differentiation, we further examined the amount of active Smad3 in mutant versus wild type. The amount of phosphorylated Smad3 is significantly increased in the rib chondrocytes of *Flnb* mutants by Western blot analysis (Fig. 5 J), although this could not be readily detected by immunostaining (Fig. S2).

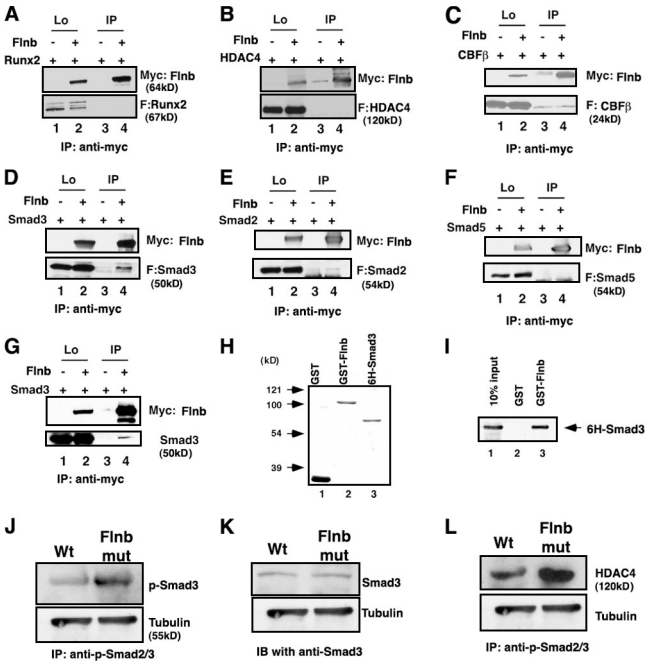

Figure 5. **Smad3 is a mediator between Filamin B and Runx2.** (A–F) Immunoprecipitation shows that the C terminus of Filamin B interacts with Smad3. Anti-myc antibody can pull down Smad3 (D), but not Runx2 (A), HDAC4 (B), CBFβ (C), Smad2 (E), or Smad5 (F) in the cotransfection protein extract (compare lanes 4 with lanes 2). Filamin B is tagged with myc, whereas Runx2, HDAC4, CBFβ, Smad2, Smad3, and Smad5 are tagged with flag. Lanes 1 and 2 are loading controls. Lanes 3 and 4 are immunoprecipitations with anti-myc antibody. Lo, loading; F, flag. (G) Recombinant myc-tagged Flnb protein immunoprecipitates endogenous Smad3 protein in 293T cells. (H) Coomassie staining shows recombinant GST, GST-tagged Flnb, and His-tagged Smad3 proteins derived from bacteria. (I) In vitro pull-down assay shows that GST-tagged Flnb directly interacts with his-tagged Smad3, whereas GST alone does not. (J) Western blot shows that there are more phosphorylated Smad3 proteins in Flnb mutants than in the wild-type cells. (K) The total amount of Smad3 protein is not changed in the mutants compared with wild-type cells. (L) Coimmunoprecipitation shows that more HDAC4 protein can be pulled down with anti–p-Smad3 antibody in Flnb mutant chondrocytes, suggesting that there are more p-Smad3–HDAC4 complexes in the Flnb mutants than in the wild type. Tubulin serves as the loading controls for the immunoprecipitations or immunoblottings.

Meanwhile, the total amount of Smad3 is not changed in the mutants (Fig. 5 K). Thus, Flnb may regulate Smad3 to ensure the accumulation of an appropriate amount of activated Smad3 in the nucleus (Fig. 6 A). An excessive amount of phosphorylated Smad3 may titrate out HDAC4, leading to a failure to form the repressive HDAC4–Smad3–Runx2 complex. In this model, amounts of HDAC4 need not to be changed (Fig. S2). In support of this model, we noticed that $Filb^{mut}$ rib chondrocytes contain more p-Smad3–HDAC4 complex than in wild-type cells because more HDAC4 can be coimmunoprecipitated by anti–p-Smad3 antibody (Fig. 5 L). The titration of HDAC4 proposed in this model may disrupt the repressive HDAC4–Smad3–Runx2 complex, resulting in the improper activation of Runx2 (Fig. 6 B).

Discussion

Together, our data show that disruption of *Flnb* leads to abnormal differentiation of chondrocytes into hypertrophic chondrocytes, causing ectopic bone formation in cartilaginous elements

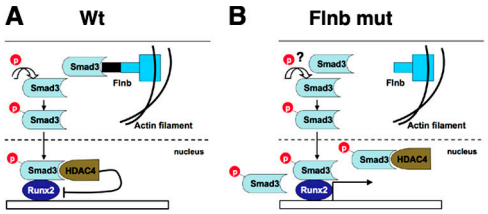

Figure 6. **A model of how Filamin B regulates chondrocyte hypertrophy.** (A) In a normal cell, the C terminus of Filamin B recruits Smad3 and prevents it from being phosphorylated. However, the unsequestrated Smad3 undergoes phosphorylation, enters the nucleus, and interacts with both Runx2 and HDAC4 to form a protein complex. As a result, HDAC4 represses Runx2 activity and inhibits the abnormal differentiation of chondrocytes into hypertrophic chondrocytes. (B) In *Flnb* mutants, the Filamin B protein lacking the C terminus cannot bind Smad3 so that possibly more Smad3 proteins are phosphorylated and enter the nucleus. In the nucleus, some of the phosphorylated Smad3 bind HDAC4, whereas others remain isolated. The isolated Smad3 proteins compete for Runx2 binding sites with the Smad3–HDAC4 complex. Thus, fewer Smad3–HDAC4 complexes bind Runx2, leading to Runx2 hyperactivity and thereby the abnormal differentiation of chondrocytes into hypertrophic chondrocytes. P, phosphorylation.

of the cervical vertebrae, carpal bone, and rib cage. That this phenotype can be rescued by inactivating one *Runx2* allele identifies an *Flnb*/*Runx2* genetic cascade regulating chondrogenesis. Thus, the regulation of Runx2 function during chondrogenesis is more complicated than previously thought.

Our data indicate that the action of Flnb on Runx2 is mediated through the TGF-β–Smad3 pathway, likely by controlling phosphorylated Smad3. Interestingly, similar to the effect of the accumulation of phosphorylated Smad3, loss of TGF-β–Smad3 signals also causes excessive chondrocyte hypertrophy (Yang et al., 2001). These seemingly contradictory results led us to propose that the homeostasis of activated Smad3 protein is essential for suppressing Runx2 activity because the readout of TGF-β depends on the amount of HDAC4–Smad3–Runx2 triple protein complex in the nucleus (Fig. 6). Consequently, either excessive Smad3 or lack of Smad3 will result in Runx2 activation. This is consistent with both the role of Smad3 in preventing chondrocyte differentiation (Ferguson et al., 2000; Yang et al., 2001; Tchetina et al., 2006) and with reports suggesting that TGF-β can up-regulate Mmp13 production in human osteoarthritic chondrocytes (Tardif et al., 1999; Moldovan et al., 2000). We remain aware that further experiments are needed to test all aspects of this model. These results do not exclude the possibility that other mechanisms also contribute to the phenotype observed in the mutant mice.

The interaction between Flnb and Smad3 in chondrocyte differentiation revealed in this study indicates that Filamins are involved in TGF-β–Smad signaling. Supporting this notion, Filamin A physically interacts with Smad2 and -5 and functionally promotes Smad2 phosphorylation, which is suggested by the lack of phosphorylation in *Filamin A*–defective human melanoma cells (Sasaki et al., 2001). Although our results indicate that Flnb normally prevents excessive Smad3 phosphorylation, we hypothesize that the action of Filamins on Smad proteins may vary in different cell types.

From a biomedical point of view, this study provides a mouse model for SSS, a disease associated with nonsense mutations in *FLNB*; more important, it uncovers a molecular mechanism explaining the vertebral and carpal bone fusions seen in these patients. In contrast to the ectopic ossification caused by nonsense mutations in *FLNB*, missense mutations in *FLNB* cause the absence or underossification of limb bones and vertebrae in Boomerang dysplasia (Bicknell et al., 2005) and atelosteogenesis I and III (Krakow et al., 2004). In these dominant disorders, we speculate that the mutant Flnb causes delayed chondrocyte hypertrophy or affects osteoblast differentiation. In fact, Flnb may also regulate Runx2 function in osteoblast differentiation, as indicated by the less developed occipital bone, which is formed through intramembranous ossification, in $Runx2^{+/-}$; $Flnb^{mut}$ than in $Runx2^{+/-}$; $Flnb^{wt}$ mice (Fig. S3, available at http://www.jcb.org/cgi/content/full/jcb.200703113/DC1). Examining more alleles of *Flnb* in the mouse will provide further insights into its additional roles in skeletal development. In summary, our study not only reveals a new mechanism for regulating chondrocyte differentiation but also provides a molecular basis for the skeletal dysplasia caused by *FLNB* nonsense mutations.

Materials and methods

Generation of mice and lines used

The *Filamin B* gene trap mice were generated with the 129/Ola ES cell line XD076 from BayGenomics (http://baygenomics.ucsf.edu/). The ES cell line was expanded and injected into C57BL/6-Albino blastocysts in the Darwin Transgenic Mouse Core facility at Baylor College of Medicine (http://imgen.bcm.tmc.edu/dtmc/). Chimeras were bred to C57BL/6 mice, and germline transmission was achieved. Mice were genotyped using Southern blotting after BglII digestion with a probe to the 5′ end of the *β-geo* insertion, which is amplified with the primer pair: filb-5southF (AACATGGCTTGCTGTGACTG) and filb-5southR (GGAGAGGGAAATCCGAAGTC). The *Runx2* knockout was used previously (Takeda et al., 2001). The primers for genotyping the *Runx2* mice are as follows: Cbfa1DB (CACGGAGCACAGGAAGTTGGG), Cbfa1DF (TGAGCGACGTGAGCCCGGTGG), and Neo3F (AAGATGGATTGCACGCAGGTTCTC). The Cbfa1DB/Neo3F primer pair amplifies the mutant allele, whereas the Cbfa1DB/Cbfa1DF primer pair amplifies the wild-type allele. For timed matings, the morning of the vaginal plug was designated E0.5. All animal protocols were approved by the Institutional Animal Care and Use Committee of Baylor College of Medicine.

RT-PCR analysis

Total RNA was prepared from liver or kidney dissected from P21 *Flnb* homozygous, heterozygous, and wild-type mice ($n = 3$ for each genotype) using RNAqueous-4PCR kit (Ambion). Transcripts were amplified using Superscript One-Step RT-PCR Systems (Invitrogen). The primers to amplify the wild-type *Flnb* transcript spanning the β-geo insertion are as follows: rtf1 (TCTTCCCACATACGATGCAA) and rtr (TCCACTACAAAGCCCACCTC). The primers to amplify the mutant transcript (fusion of *Flnb* and *β-geo* insertion) are as follows: rtf2 (CCTATATCCCTGATAAGACCGGACGC) and gal (GACAGTATCGGCCTCAGGAAGATCG).

Skeletal preparation

Mice were dissected, fixed in 95% ethanol overnight, and stained in 0.015% alcian blue (Sigma-Aldrich) dye overnight. The carcasses were treated with 2% KOH for 1 to several days until most soft tissue disappeared. After removing the remaining soft tissues carefully with forceps, the mice were stained in 0.005% alizarin red (Sigma-Aldrich) solution for 30 min to several hours depending on the age of the mice. Finally, skeletons were cleared in a 20% glycerol/1% KOH solution. At least four mice of each genotype were analyzed for each stage.

β-Galactosidase assay

Mice at P0 were dissected so that most tissues other than skeleton are removed. The skeletons were fixed in 0.2% glutaraldehyde for 1 h at RT followed by washing in PBS twice. Fixed specimens were then put in fresh staining solution overnight at RT. The staining solution was made by mixing 1 ml 10× stock solution, 250 μl 0.2 M EGTA, and 250 μl 40 mg/ml X-gal

into 8.5 ml PBS. The 10× stock solution was made as follows: for 100 ml solution, add 1.646 g $K_4Fe(CN)_6$ Ferro, 2.112 g $K_3Fe(CN)_6$ Ferri, 2 ml 1 M $MgCl_2$, 2 ml 1% NP40, and 0.01 g sodium deoxycholate. X-gal stock solution was made by dissolving 100 mg X-gal in 2.5 ml dimethylformamide. All microscopy for skeletal preparation and X-gal staining of the skeleton are performed with Stemi SV11 microscopy (Carl Zeiss MicroImaging, Inc.) with 0.5× (Plan) and 1.0× (Planapo) objectives at RT. Pictures were taken with a color video camera (DXC 300 3CCD; Sony), captured through the Spot software (Diagnostic Instruments), and further processed with Photoshop (Adobe).

Histology and in situ hybridization

Tissues were fixed in 4% paraformaldehyde/PBS overnight at 4°C. Mice obtained after P0 were decalcified in TBD-2 solution (Thermo Shandon) overnight at 4°C. Specimens were dehydrated and embedded in paraffin and sectioned at 5 μm. For histological analysis, sections were stained with hematoxylin and eosin. In situ hybridization was performed using digoxigenin-labeled riboprobes (Roche). The α1(I), α1(II), and α1(X) probes were used previously (Takeda et al., 2001). Hybridizations were performed overnight at 60°C, and washes were performed at 65°C. Sections were then incubated for 2 h with alkaline phosphatase–linked anti-digoxigenin antibody (1:2,000; Roche) at RT followed by color reactions with BM purple substrate (Roche). Sections were finally counterstained with nuclear fast red (Vector Laboratories) and mounted with Permount. Three mice of each genotype were analyzed for each stage. The microscopy for all histology and in situ sections were performed using a microscope (AxioPlan2; Carl Zeiss MicroImaging, Inc.) with 5× (Plan-Neofluar), 10× (Plan-Apochromat), or 20× (Plan-Apochromat) objectives at RT. All images were taken with AxioCam (Carl Zeiss MicroImaging, Inc.), captured through the AxioVision software (Carl Zeiss MicroImaging, Inc.), and processed with Photoshop software (Adobe).

Plasmid construction

Smad-expressing mammalian plasmids were provided by K. Watanabe (National Institute for Longevity Sciences, Aichi, Japan; pF:Smad1, -2, -4, -5, and -6) and R. Derynck (University of California, San Francisco, San Francisco, CA; flag-Smad3; Sasaki et al., 2001; Kang et al., 2005). The CBFβ-expressing plasmid was obtained from T. Watanabe (Tohoku University, Sendai, Japan; Yoshida et al., 2005). To generate myc-tagged N terminus–truncated mammalian-expressing Filamin B, the C-terminal 231-amino-acid coding region was generated by PCR and inserted into the StuI–XbaI sites of the CS2+MT vector. To produce his-tagged Smad3 protein, PCR-amplified Smad3 gene was subcloned into NdeI and BamHI sites of a bacterial expression vector, pET-15b (Novagen). To produce GST fusion protein, the C terminus of Filamin B was PCR amplified and subcloned into NdeI and HindIII sites of a pGEX2TL.

Recombinant protein purification

BL21-pLysS was transformed with His-tagged Smad3 and GST-fused Filamin B bacterial expression vectors, respectively. After induction with IPTG, the bacterial pellets were lysed by sonication in the presence of Ni-column binding buffer (20 mM TrisCl, pH 7.9, 500 mM NaCl, and 5 mM Imidazole) and GST binding buffer (20 mM TrisCl, pH 7.9, 1 M NaCl, 0.2 mM EDTA, 2 mM DTT, and 10% Glycerol), respectively, and centrifugation was followed. From each supernatant, His-tagged Smad3 and GST-fused Filamin B proteins were isolated by Ni-NTA (GE Healthcare) chromatography and glutathione-coupled Sepharose (GE Healthcare) chromatography.

GST pull-down assays

5 mg of purified His-tagged Smad3 protein was incubated with either 10 mg immobilized GST or GST-fused Filamin B on glutathione-coupled Sepharose in BC300 (20 mM Tris, pH 7.9, 0.2 mM EDTA, 300 mM KCl, 20% glycerol, 0.1% NP-40, and 1 mM PMSF) solution containing 2 mg/ml BSA for 6 h at 4°C. The immobilized GST or GST-fused Filamin B beads were washed extensively with BC300 and analyzed by immunoblot after SDS-PAGE.

Immunoprecipitation and immunoblotting

For the immunoprecipitation and immunoblotting for the interaction between overexpressed Filamin B and overexpressed Smad3, 293T cells were cotransfected with myc-tagged Flnb and flag-tagged Runx2, HDAC4, CBFβ, and Smad proteins, respectively, using Lipofectamine 2000 (Invitrogen) according to the manufacturer's manual. 48 h later, cells were harvested and washed once with cold PBS. The cell pellet was suspended and lysed by adding 10 times the volume of hypotonic buffer. The hypotonic buffer is composed of 50 mM Tris-Cl, pH 7.5, 2 mM EDTA, 0.1% NP-40, 1 mM PMSF, and phosphatase inhibitors. The lysates were subjected to immunoprecipitation with anti-myc antibody (Santa Cruz Biotechnology, Inc.) and protein A agarose overnight, followed by Western blotting with anti-myc and anti-Flag (Sigma-Aldrich) antibodies.

For the immunoprecipitation and immunoblotting for the interaction between overexpressed Filamin B and endogenous Smad3, 293T cells transfected with myc-tagged Filamin B expression vector using Lipofectamine 2000 (Invitrogen) according to the manufacturer's manual. 48 h later, cells were harvested and washed once with PBS. The cell pellet was lysed by adding 10 times more hypotonic buffer than the pellet volume and resuspending the pellet. The hypotonic buffer is composed of 50 mM Tris-Cl, pH 7.5, 2 mM EDTA, 0.1% NP-40, 1 mM PMSF, and phosphatase inhibitors. The lysates were subjected to immunoprecipitation with anti-myc antibody and protein A agarose for overnight, followed by Western blotting with anti-myc and -Smad3 (Upstate Biotechnology) antibodies.

For the detection of p-Smad3 level and coimmunoprecipitation of p-Smad3 and HDAC4, cartilaginous tissues from Rib cages of wild-type and Filamin B mutant mice at P4 were homogenized in 500 ml lysis buffer using a tissue miser (Tekmar). The lysis buffer is composed of 50 mM Tris, pH 7.5, 2 mM EDTA, 150 mM NaCl, 1% Triton X-100, and protease and phosphatase inhibitor cocktail. These lysates were subjected to immunoprecipitation with anti–phospho-Smad2/3 antibody (Santa Cruz Biotechnology, Inc.) and protein A agarose for 6 h, followed by immunoblotting with anti-Smad3 and anti-HDAC4 (Santa Cruz Biotechnology, Inc.) antibody. As an input control of the immunoprecipitation, the lysates were subjected to immunoblotting with anti-tubulin antibody (Santa Cruz Biotechnology, Inc.).

Online supplemental material

Fig. S1 shows the expression of different portions of the *Filamin B* transcript in the mutant compared with the wild type. Fig. S2 shows the expression of CBFβ, HDAC4, p-Smad3, and Runx2 in the chondrocytes and interaction between Filamin B and Smad4 or -6. Fig. S3 shows the aggravated occipital bone phenotype by deleting *Filamin B* in the background of *Runx2* haploinsufficiency. Online supplemental material is available at http://www.jcb.org/cgi/content/full/jcb.200703113/DC1.

We thank Drs. Patricia Ducy, Richard Behringer, and Brendan Lee for critically reviewing the manuscript.

This work was supported by Public Health Service grants P01 ES11253 and U01 HD39372, by a gift from the Kleberg Foundation to M.J. Justice, and by The National Institute of Arthritis and Musculoskeletal and Skin Diseases grant R01 AR 045548 to G. Karsenty.

Submitted: 19 March 2007
Accepted: 5 June 2007

References

Bialek, P., B. Kern, X. Yang, M. Schrock, D. Sosic, N. Hong, H. Wu, K. Yu, D.M. Ornitz, E.N. Olson, et al. 2004. A twist code determines the onset of osteoblast differentiation. *Dev. Cell.* 6:423–435.

Bicknell, L.S., T. Morgan, L. Bonafe, M.W. Wessels, M.G. Bialer, P.J. Willems, D.H. Cohn, D. Krakow, and S.P. Robertson. 2005. Mutations in FLNB cause boomerang dysplasia. *J. Med. Genet.* 42:e43.

Ducy, P., R. Zhang, V. Geoffroy, A.L. Ridall, and G. Karsenty. 1997. Osf2/Cbfa1: a transcriptional activator of osteoblast differentiation. *Cell.* 89:747–754.

Farrington-Rock, C., M.H. Firestein, L.S. Bicknell, A. Superti-Furga, C.A. Bacino, V. Cormier-Daire, M. Le Merrer, C. Baumann, J. Roume, P. Rump, et al. 2006. Mutations in two regions of FLNB result in atelosteogenesis I and III. *Hum. Mutat.* 27:705–710.

Feng, Y., and C.A. Walsh. 2004. The many faces of filamin: a versatile molecular scaffold for cell motility and signalling. *Nat. Cell Biol.* 6:1034–1038.

Ferguson, C.M., E.M. Schwarz, P.R. Reynolds, J.E. Puzas, R.N. Rosier, and R.J. O'Keefe. 2000. Smad2 and 3 mediate transforming growth factor-beta1-induced inhibition of chondrocyte maturation. *Endocrinology.* 141:4728–4735.

Hinoi, E., P. Bialek, Y.T. Chen, M.T. Rached, Y. Groner, R.R. Behringer, D.M. Ornitz, and G. Karsenty. 2006. Runx2 inhibits chondrocyte proliferation and hypertrophy through its expression in the perichondrium. *Genes Dev.* 20:2937–2942.

Kang, J.S., T. Alliston, R. Delston, and R. Derynck. 2005. Repression of Runx2 function by TGF-beta through recruitment of class II histone deacetylases by Smad3. *EMBO J.* 24:2543–2555.

Karsenty, G., and E.F. Wagner. 2002. Reaching a genetic and molecular understanding of skeletal development. *Dev. Cell.* 2:389–406.

Komori, T. 2002. Runx2, a multifunctional transcription factor in skeletal development. *J. Cell. Biochem.* 87:1–8.

Komori, T. 2006. Regulation of osteoblast differentiation by transcription factors. *J. Cell. Biochem.* 99:1233–1239.

Krakow, D., S.P. Robertson, L.M. King, T. Morgan, E.T. Sebald, C. Bertolotto, S. Wachsmann-Hogiu, D. Acuna, S.S. Shapiro, T. Takafuta, et al. 2004. Mutations in the gene encoding filamin B disrupt vertebral segmentation, joint formation and skeletogenesis. *Nat. Genet.* 36:405–410.

Kronenberg, H.M. 2004. Twist genes regulate Runx2 and bone formation. *Dev. Cell.* 6:317–318.

Moldovan, F., J.P. Pelletier, F. Mineau, M. Dupuis, J.M. Cloutier, and J. Martel-Pelletier. 2000. Modulation of collagenase 3 in human osteoarthritic cartilage by activation of extracellular transforming growth factor beta: role of furin convertase. *Arthritis Rheum.* 43:2100–2109.

Popowicz, G.M., M. Schleicher, A.A. Noegel, and T.A. Holak. 2006. Filamins: promiscuous organizers of the cytoskeleton. *Trends Biochem. Sci.* 31:411–419.

Robertson, S.P., S.R. Twigg, A.J. Sutherland-Smith, V. Biancalana, R.J. Gorlin, D. Horn, S.J. Kenwrick, C.A. Kim, E. Morava, R. Newbury-Ecob, et al. 2003. Localized mutations in the gene encoding the cytoskeletal protein filamin A cause diverse malformations in humans. *Nat. Genet.* 33:487–491.

Sakou, T., T. Onishi, T. Yamamoto, T. Nagamine, T. Sampath, and P. Ten Dijke. 1999. Localization of Smads, the TGF-beta family intracellular signaling components during endochondral ossification. *J. Bone Miner. Res.* 14:1145–1152.

Sasaki, A., Y. Masuda, Y. Ohta, K. Ikeda, and K. Watanabe. 2001. Filamin associates with Smads and regulates transforming growth factor-beta signaling. *J. Biol. Chem.* 276:17871–17877.

Stossel, T.P., J. Condeelis, L. Cooley, J.H. Hartwig, A. Noegel, M. Schleicher, and S.S. Shapiro. 2001. Filamins as integrators of cell mechanics and signalling. *Nat. Rev. Mol. Cell Biol.* 2:138–145.

Takeda, S., J.P. Bonnamy, M.J. Owen, P. Ducy, and G. Karsenty. 2001. Continuous expression of Cbfa1 in nonhypertrophic chondrocytes uncovers its ability to induce hypertrophic chondrocyte differentiation and partially rescues Cbfa1-deficient mice. *Genes Dev.* 15:467–481.

Tardif, G., J.P. Pelletier, M. Dupuis, C. Geng, J.M. Cloutier, and J. Martel-Pelletier. 1999. Collagenase 3 production by human osteoarthritic chondrocytes in response to growth factors and cytokines is a function of the physiologic state of the cells. *Arthritis Rheum.* 42:1147–1158.

Tchetina, E.V., J. Antoniou, M. Tanzer, D.J. Zukor, and A.R. Poole. 2006. Transforming growth factor-beta2 suppresses collagen cleavage in cultured human osteoarthritic cartilage, reduces expression of genes associated with chondrocyte hypertrophy and degradation, and increases prostaglandin E(2) production. *Am. J. Pathol.* 168:131–140.

van der Flier, A., and A. Sonnenberg. 2001. Structural and functional aspects of filamins. *Biochim. Biophys. Acta.* 1538:99–117.

Vega, R.B., K. Matsuda, J. Oh, A.C. Barbosa, X. Yang, E. Meadows, J. McAnally, C. Pomajzl, J.M. Shelton, J.A. Richardson, et al. 2004. Histone deacetylase 4 controls chondrocyte hypertrophy during skeletogenesis. *Cell.* 119:555–566.

Yang, X., L. Chen, X. Xu, C. Li, C. Huang, and C.X. Deng. 2001. TGF-beta/Smad3 signals repress chondrocyte hypertrophic differentiation and are required for maintaining articular cartilage. *J. Cell Biol.* 153:35–46.

Yoshida, C.A., H. Yamamoto, T. Fujita, T. Furuichi, K. Ito, K. Inoue, K. Yamana, A. Zanma, K. Takada, Y. Ito, and T. Komori. 2004. Runx2 and Runx3 are essential for chondrocyte maturation, and Runx2 regulates limb growth through induction of Indian hedgehog. *Genes Dev.* 18:952–963.

Yoshida, N., T. Ogata, K. Tanabe, S. Li, M. Nakazato, K. Kohu, T. Takafuta, S. Shapiro, Y. Ohta, M. Satake, and T. Watanabe. 2005. Filamin A-bound PEBP2beta/CBFbeta is retained in the cytoplasm and prevented from functioning as a partner of the Runx1 transcription factor. *Mol. Cell. Biol.* 25:1003–1012.

Zhang, D., J.A. Herring, S.S. Swaney, T.B. McClendon, X. Gao, R.H. Browne, K.E. Rathjen, C.E. Johnston, S. Harris, N.M. Cain, and C.A. Wise. 2006. Mutations responsible for Larsen syndrome cluster in the FLNB protein. *J. Med. Genet.* 43:e24.